

**SUBMERGED VACUUM MEMBRANE
DISTILLATION (S-VMD) FOR MARINE
AQUACULTURE WATER DESALINATION**

CHANG YING SHI

UNIVERSITI SAINS MALAYSIA

2021

**SUBMERGED VACUUM MEMBRANE DISTILLATION (S-VMD) FOR
MARINE AQUACULTURE WATER DESALINATION**

by

CHANG YING SHI

**Thesis submitted in fulfilment of the
requirements for the degree of
Doctor of Philosophy**

June 2021

ACKNOWLEDGEMENT

I would like to acknowledge my supervisor, Prof. Dr. Ooi Boon Seng as well as my two co-supervisors, Prof. Ir. Dr. Abdul Latif and Assoc. Prof. Ir. Dr. Leo Choe Peng, for playing pivotal role towards the completion of my degree of Doctor of Philosophy. I have received a lot of invaluable knowledges, guidance and numerous consultations from them. Their enthusiasm and creativity for research in membrane field are contagious. I would also like to acknowledge the financial support of Transdisciplinary Research Grant Scheme (TRGS) (TRGS/1/2018/USM/01/5/2) (203.PJKIMIA/67612002) from the Ministry of Higher Education Malaysia throughout my research study.

I am grateful to Mr. Shamsul Hidayat Shaharan for helping me in setting up the experimental submerged vacuum membrane distillation system. I am always amazed of his knowledges and hands-on technical skill. I have received an array of noble advices that are useful to solve the operational problems during running experiments and make my research success. A special gratitude also goes out to all technical and administrative staffs in the School of Chemical Engineering, Universiti Sains Malaysia for their countless help throughout my research study.

I am also grateful to my parents who have always been extremely helpful in supporting my education. My siblings have always been a source of inspiration in my life. I am truly thankful for their moral support. Last but not least, in completing of my Ph.D study, I had to receive the endless help of my dearest friends, who deserve my greatest gratitude; Lyly, Imani, Wei Ming, Dr. Beh, Dr. Aini, Dr Atiah, Yi Tong, Yin Sim, Aaron, Syamimi, Allia and Mariam.

TABLE OF CONTENTS

| | |
|--|--------------|
| ACKNOWLEDGEMENT | ii |
| TABLE OF CONTENTS | iii |
| LIST OF TABLES | viii |
| LIST OF FIGURES | ix |
| LIST OF SYMBOLS | xvii |
| LIST OF ABBREVIATIONS | xxi |
| LIST OF APPENDICES | xxiii |
| ABSTRAK | xxiv |
| ABSTRACT | xxvi |
| CHAPTER 1 INTRODUCTION | 1 |
| 1.1 Research background | 1 |
| 1.2 Problem statements | 5 |
| 1.3 Research objectives | 8 |
| 1.4 Scope of study | 9 |
| 1.5 Thesis organization | 10 |
| CHAPTER 2 LITERATURE REVIEW | 13 |
| 2.1 Marine aquaculture..... | 13 |
| 2.2 Application of VMD for desalination | 15 |
| 2.2.1 Principle of VMD..... | 15 |
| 2.2.2 Conventional and submerged VMD configurations used in desalination..... | 16 |
| 2.3 Fouling phenomenon in MD | 21 |
| 2.3.1 Inorganic fouling | 23 |
| 2.3.2 Organic fouling | 26 |
| 2.3.3 Biofouling..... | 28 |

| | | |
|-----------------------------------|---|-----------|
| 2.4 | Fouling control strategies in MD | 31 |
| 2.4.1 | Operational parameters | 31 |
| 2.4.1(a) | Feed temperature | 31 |
| 2.4.1(b) | Feed velocity..... | 32 |
| 2.4.1(c) | Applied pressure | 32 |
| 2.4.2 | Processing aid via bubbling..... | 34 |
| 2.5 | Energy consumption of conventional and submerged VMD for desalination | 36 |
| 2.6 | Desalination of marine aquaculture water using S-VMD | 39 |
| 2.7 | Research gaps | 40 |
| CHAPTER 3 METHODOLOGY..... | | 43 |
| 3.1 | Materials and chemicals | 43 |
| 3.1.1 | Materials..... | 43 |
| 3.1.2 | Chemicals | 45 |
| 3.1.3 | Apparatus | 48 |
| 3.2 | Experimental procedures | 53 |
| 3.2.1 | Experimental flow chart..... | 53 |
| 3.2.2 | Jar test study | 54 |
| 3.2.3 | Numerical study of S-VMD model | 55 |
| 3.2.3(a) | Mass transfer mechanism in S-VMD | 55 |
| 3.2.3(b) | Heat transfer mechanism in S-VMD | 57 |
| 3.2.3(c) | Economic analysis of S-VMD model | 62 |
| 3.2.3(d) | Numerical simulation of S-VMD model | 63 |
| 3.2.4 | S-VMD experimental setup..... | 66 |
| 3.2.5 | Marine algae culture..... | 70 |
| 3.2.6 | Bubble movement and size characterization..... | 72 |
| 3.3 | Membrane characterization | 75 |
| 3.3.1 | Chemical fixation on microalgal fouled membranes | 75 |

| | | |
|--|--|-----------|
| 3.3.2 | Scanning electron microscopy and energy dispersive X-ray (SEM-EDX) | 75 |
| 3.3.3 | X-Ray diffraction (XRD) | 76 |
| 3.3.4 | High resolution transmission electron microscopy (HRTEM) | 77 |
| 3.3.5 | Attenuated total reflectance Fourier transform infrared (ATR-FTIR)..... | 77 |
| 3.3.6 | Water contact angle measurement..... | 77 |
| 3.3.7 | Capillary flow porometry | 78 |
| 3.3.8 | Exopolymeric substances (EPS) extraction..... | 79 |
| 3.3.9 | Zeta potential measurement | 80 |
| 3.3.10 | Atomic Force Microscopy (AFM) | 80 |
| 3.4 | Water quality analysis for feed and permeate | 81 |
| 3.4.1 | Atomic Absorption Spectrometry (AAS)..... | 81 |
| 3.4.2 | Total suspended solids (TSS)..... | 81 |
| 3.4.3 | Mixed liquor volatile suspended solids (MLVSS)..... | 82 |
| 3.4.4 | Total organic carbon (TOC)..... | 82 |
| 3.4.5 | pH, salinity and conductivity measurements..... | 83 |
| 3.4.6 | Photometric measurements | 83 |
| 3.5 | Economic analysis of air bubbling enhanced S-VMD system..... | 84 |
| 3.5.1 | Total power input and specific energy consumption (<i>SEC</i>) of air bubbling enhanced S-VMD system | 84 |
| 3.5.2 | Gained output ratio (<i>GOR</i>) of air bubbling enhanced S-VMD system..... | 84 |
| CHAPTER 4 RESULTS AND DISCUSSION..... | | 86 |
| 4.1 | Preliminary study | 86 |
| 4.1.1 | Jar test study | 86 |
| 4.1.1(a) | Structural characteristics of single scalant at elevated feed temperature | 86 |
| 4.1.1(b) | Structural characteristics of mixed scalants at elevated feed temperature | 92 |

| | | |
|----------|--|-----|
| 4.1.1(c) | Membrane fouling at elevated temperature of marine aquaculture water | 93 |
| 4.1.2 | Short term S-VMD experiments for membrane selection..... | 100 |
| 4.1.2(a) | S-VMD experiments for pure and saline water | 100 |
| 4.1.2(b) | S-VMD experiments for marine aquaculture water and membrane scaling study..... | 102 |
| 4.2 | Analysis of system performance via numerical study | 108 |
| 4.2.1 | Analysis of system performance at different feed temperature and circulation flow rates | 108 |
| 4.2.2 | Analysis of System Performance at different permeate pressure for varied feed temperature and feed circulation | 112 |
| 4.2.3 | Performance projection | 114 |
| 4.2.3(a) | Analysis of system performance at projected feed temperature and circulation flow rates | 114 |
| 4.2.3(b) | Analysis of system performance at projected number of hollow fibres and circulation rates | 115 |
| 4.3 | Membrane fouling control strategy by air bubbling..... | 120 |
| 4.3.1 | Air bubbling on membrane scaling control..... | 120 |
| 4.3.1(a) | Efficiency of scaling control by air bubbling | 121 |
| 4.3.1(b) | Analysis of air bubbling fouling control effect on the membrane surface | 127 |
| 4.3.2 | Bubble flow observation | 136 |
| 4.3.2(a) | Bubble characteristics | 136 |
| 4.3.2(b) | Bubble flow velocities and its trajectory | 137 |
| 4.3.2(c) | Shear stress calculation..... | 139 |
| 4.3.2(d) | Theoretical analysis of the hydrodynamic forces exerted on the foulants under different air flow rates | 140 |
| 4.3.3 | Air bubbling for organic fouling control..... | 142 |
| 4.3.3(a) | Performance analysis of air bubbling for organic fouling control | 142 |
| 4.3.3(b) | Microalgal fouling characterization..... | 143 |

| | | |
|--|---|------------|
| 4.4 | Bubbling aided S-VMD system for marine aquaculture water desalination | 158 |
| 4.4.1(a) | Range of quality parameters of marine aquaculture water | 158 |
| 4.4.1(b) | Evaluation on long term flux performance and fouling control | 159 |
| 4.4.1(c) | Membrane characterization | 161 |
| 4.5 | Energy efficiency of air bubbling enhanced S-VMD system..... | 167 |
| 4.5.1(a) | Analysis of total energy consumption and <i>SEC</i> under different bubbling modes and bubble flow..... | 167 |
| 4.5.1(b) | Analysis of <i>GOR</i> of the air bubbling enhanced S-VMD system..... | 169 |
| CHAPTER 5 CONCLUSION AND FUTURE RECOMMENDATIONS.... | | 171 |
| 5.1 | Conclusion..... | 171 |
| 5.2 | Recommendations for future research..... | 175 |
| REFERENCES..... | | 177 |
| APPENDICES | | |
| LIST OF PUBLICATIONS | | |

LIST OF TABLES

| | Page |
|-----------|---|
| Table 2.1 | Published literature reports about the application of VMD and S-VMD configurations in desalination..... 17 |
| Table 3.1 | The parameters of commercial PP hollow fibre membrane bundle that used in S-VMD experiments.....44 |
| Table 3.2 | The quality parameters of marine aquaculture water.....45 |
| Table 3.3 | List of chemicals used in this study.45 |
| Table 3.4 | Apparatus and instruments used.50 |
| Table 4.1 | EDX elemental analysis results of MgSO ₄ scalant on membrane surface of (a) ZENA PP and (b) ACCUREL PP at feed temperature range of 298 to 343 K.....91 |
| Table 4.2 | EDX elemental analysis results of the scalants formation on the membrane surface of (a) ZENA PP and (b) ACCUREL PP using marine aquaculture water as feed solution with temperature range of 298 to 343 K. 100 |
| Table 4.3 | Comparison of the current S-VMD performance with other conventional VMD literatures..... 118 |
| Table 4.4 | Summary of the calculated shear stress exerted on the membrane surface at different air flow rates. 139 |
| Table 4.5 | Quality parameters of marine aquaculture water varies in 2019 and 2020..... 158 |
| Table 4.6 | Quality parameters of permeate over 344 h air bubbling S-VMD operation..... 160 |

LIST OF FIGURES

| | Page |
|-------------|---|
| Figure 2.1 | Types of membrane fouling in MD process.....23 |
| Figure 3.1 | Marine aquaculture water sampling site.44 |
| Figure 3.2 | S-VMD experimental set-up.....48 |
| Figure 3.3 | Experimental flow chart of this project.54 |
| Figure 3.4 | Tube pitch between adjacent hollow fibres in the square pitch arrangement.....59 |
| Figure 3.5 | S-VMD simulation flow chart.65 |
| Figure 3.6 | Schematic diagram of S-VMD process in the mode of (a) stagnant, (b) circulation and (c) bubbling.66 |
| Figure 3.7 | Membrane bundle used in S-VMD experiments.67 |
| Figure 3.8 | Microscopic image of <i>Cylindrotheca fusiformis sp.</i> with the cell density of approximately 1.5×10^5 cells/mL at room temperature (magnification: 20x).....71 |
| Figure 3.9 | The experimental set-up for bubble flow image capture.72 |
| Figure 3.10 | Mechanism of air bubbling in the scaling mitigation with different forces experienced by the foulants on the membrane surface under the impact of shear rates from air bubbles.74 |
| Figure 3.11 | The arithmetic mean of contact angle measured by goniometer.78 |
| Figure 4.1 | SEM images of (a) pristine membranes: ZENA PP (left) and ACCUREL PP (right), MgCO ₃ scalants on the (b) ZENA PP and (c) ACCUREL PP membrane surface and MgSO ₄ scalants on (d) ZENA PP and (e) ACCUREL PP membrane surface at feed temperatures of 298 K (left side) and 343 K (right side): magnification: 5,000x (feed stirring speed: 100 rpm, running time: 72 h).88 |

| | | |
|------------|--|----|
| Figure 4.2 | SEM images of single MgSO ₄ scalant formed on the membrane surface of ZENA PP (left side) and ACCUREL PP (right side) at (a) 298 K, (b) 313 K, (c) 323 K, (d) 333 K, (e) 343 K, respectively (magnification: 5,000x)..... | 90 |
| Figure 4.3 | SEM images of mixed magnesium deposits on (a) ZENA PP and (b) ACCUREL PP membrane surface in mixed scaling experiment at feed temperature of 298 K (left) and 343 K (right) (magnification: 5,000x, feed stirring speed: 100 rpm, running time: 72 h). | 92 |
| Figure 4.4 | SEM images with elemental analysis of the scalants found on (a) ZENA PP membrane surface (b) ZENA PP cross-section (c) ACCUREL PP membrane surface and (d) ACCUREL PP cross-section using marine aquaculture water in scaling jar test at 343 K (magnification: 5,000x)..... | 93 |
| Figure 4.5 | TEM image of deposits formed on the cross section of the ZENA PP membrane using marine aquaculture water as feed solution at 343 K (magnification: 19,500×) (feed stirring speed: 100 rpm, running time: 72 h)..... | 95 |
| Figure 4.6 | Results of TEM-EDX analysis of elemental deposits (a) Mg (b) O (c) Si (d) S and (e) C formed on the cross-section of the ZENA PP membrane using marine aquaculture water as feed at 343 K (magnification: 19,500×) (feed stirring speed: 100 rpm, running time: 72 h). | 95 |
| Figure 4.7 | XRD patterns of magnesium based foulants formed on the ZENA PP membrane using marine aquaculture water as feed at 298 K and 343 K, respectively (feed stirring speed: 100 rpm, running time: 72 h). | 96 |
| Figure 4.8 | FTIR analysis of pristine and fouled ZENA PP membranes using marine aquaculture water as feed at temperature of 298 K and 343 K, respectively (feed stirring speed: 100 rpm, running time: 72 h)... | 98 |
| Figure 4.9 | SEM images of magnesium based deposits formed on membrane surface of ZENA PP (left side) and ACCUREL PP (right side) | |

| | | |
|-------------|--|-----|
| | using marine aquaculture water as feed solution at (a) 298 K, (b) 313 K, (c) 323 K, (d) 333 K (e) 343 K, respectively (magnification: 5,000x). | 99 |
| Figure 4.10 | Average (a) pure water and (b) saline water flux for S-VMD with the two commercial PP hollow fibres at operating temperatures of 328 and 333 K at 3 kPa over 3 h of operation..... | 101 |
| Figure 4.11 | (a) Time variation marine aquaculture water flux and (b) Feed concentration for S-VMD with the two commercial PP hollow fibres at operating temperatures of 328 and 333 K at 3 kPa over 12 h of operation. | 102 |
| Figure 4.12 | SEM-EDX analysis of Mg-based and NaCl deposits formed on membrane surface of ZENA PP (left side) and ACCUREL PP (right side) after 12 h VMD operation under 3 kPa using marine aquaculture water as feed at (a) 328 and (b) 333 K (magnification: 5,000×). | 103 |
| Figure 4.13 | Pore size distribution of ZENA PP and ACCUREL PP membranes for fresh condition and after 12 h of S-VMD operation at different feed temperatures. | 106 |
| Figure 4.14 | TEM image of deposits formed on the cross section of (a) ZENA PP (b) ACCUREL PP membranes after 12 h of S-VMD operation at 333 K under 3 kPa using marine aquaculture water as feed (magnification: 19,500×)..... | 107 |
| Figure 4.15 | System performance of S-VMD with respect to permeate flux, temperature polarization (<i>TPC</i>), heat transfer coefficient and temperature difference of the coil that provide the transmembrane mass transfer (ΔT_{coil}) as a function of varied feed temperature and circulation rate at constant vacuum pressure 3 kPa absolute for the four hollow fibres. (Lines: Simulation results; Points: Experimental results) | 109 |
| Figure 4.16 | The predicted gained output ratio (<i>GOR</i>) as a function of feed temperature at different circulation rate and (b) Circulation pump energy input for water production at constant feed temperature of | |

| | | |
|-------------|--|-----|
| | 333 K, respectively under constant vacuum pressure of 3 kPa absolute for the S-VMD system using four hollow fibres. | 111 |
| Figure 4.17 | Permeate flux as a function of (a) varied vacuum pressure and feed temperature at fixed circulation rate of 0.9 L/min and (b) varied vacuum pressure and feed circulation at fixed feed temperature at 333 K for the S-VMD system using four hollow fibres. (Lines: Simulation results; Points: Experimental results) | 112 |
| Figure 4.18 | The predicted <i>GOR</i> and <i>SEC</i> as a function of (a) varied vacuum pressure and feed temperature at fixed circulation rate of 0.9 L/min and (b) varied vacuum pressure and circulation flow at fixed feed temperature of 333 K for the S-VMD system using four hollow fibres..... | 113 |
| Figure 4.19 | The simulated <i>GOR</i> and <i>SEC</i> versus varied feed temperature at different circulation rates under constant vacuum pressure of 3 kPa absolute for the S-VMD system using four hollow fibres. | 114 |
| Figure 4.20 | <i>TPC</i> and heat transfer coefficient as a function of (a) varied number of the PP hollow fibres used at feed circulation of 2.1 L/min and (b) varied feed circulation flow using 40 hollow fibres, respectively under fixed feed temperature of 353 K and permeate pressure at 3 kPa absolute. | 115 |
| Figure 4.21 | Predicted <i>GOR</i> and <i>SEC</i> as a function of varied number of the PP hollow fibres and circulation flow at fixed feed temperature of 353 K and permeate pressure at 3 kPa absolute..... | 117 |
| Figure 4.22 | (a) Flux patterns and (b) normalized flux achieved for the S-VMD experiments over 40 h using a feed solution of 4.07 g/L Na ₂ SO ₄ + 5.84 g/L MgCl ₂ in 2.0 wt.% NaCl (left) and 3.5 wt.% NaCl (right) at 333 K under intermittent and continuous modes of various air flow rates and circulation mode. Normalized flux is the ratio of the instant flux to the initial flux..... | 121 |
| Figure 4.23 | SEM-EDX analysis of the membrane surface after 40 h running S-VMD using 4.07 g/L Na ₂ SO ₄ + 5.84 g/L MgCl ₂ in 2.0 wt.% NaCl (above) and 3.5 wt.% NaCl (bottom) as feed at temperature of 333 | |

| | | |
|-------------|---|-----|
| | K under the mode of (a) stagnant, (b) circulation at 0.9 L/min, (c) continuous bubbling at 30 L/min, (d) intermittent bubbling at 30 L/min, (e) continuous bubbling at 60 L/min, and (f) intermittent bubbling at 60 L/min (magnification: 5,000×)..... | 124 |
| Figure 4.24 | SEM images of cross section of the used membrane after 40 h running S-VMD using 4.07 g/L Na ₂ SO ₄ + 5.84 g/L MgCl ₂ in 2.0 wt.% NaCl (left) and 3.5 wt.% NaCl (right) as feed at temperature of 333 K under the mode of (a) stagnant, (b) circulation at 0.9 L/min, (c) continuous bubbling at 30 L/min, (d) intermittent bubbling at 30 L/min, (e) continuous bubbling at 60 L/min, and (f) intermittent bubbling at 60 L/min (magnification: 5,000×). | 129 |
| Figure 4.25 | FTIR analysis of the pristine and scaled hollow fibres after 40 h running S-VMD using 4.07 g/L Na ₂ SO ₄ + 5.84 g/L MgCl ₂ in 2.0 wt.% NaCl (top) and 3.5 wt.% NaCl (bottom) as feed at temperature of 333 K under the mode of stagnant, circulation, intermittent and continuous bubbling at 30 and 60 L/min. | 131 |
| Figure 4.26 | XRD spectra of magnesium sulphate scaled on the hollow fibres after 40 h running S-VMD using 4.07 g/L Na ₂ SO ₄ + 5.84 g/L MgCl ₂ in 2.0 wt.% NaCl (top) and 3.5 wt.% NaCl (bottom) as feed at temperature of 333 K under the mode of stagnant, circulation, intermittent and continuous bubbling at 30 and 60 L/min. | 133 |
| Figure 4.27 | Pore size distribution of the pristine and used membranes after 40 h of air bubbling enhanced S-VMD operation using 4.07 g/L Na ₂ SO ₄ + 5.84 g/L MgCl ₂ in 2.0 wt.% NaCl (top) and 3.5 wt.% NaCl (bottom) as feed. | 135 |
| Figure 4.28 | The bubble flow images captured at different air flow rates, (a) 30 L/min, (b) 60 L/min with vacuum (right) and without vacuum (left) conditions. (frame rate: 400 fps) | 136 |
| Figure 4.29 | The images of bubble trajectory at different air flow rates, (a) 30 L/min, (b) 60 L/min under vacuum condition in every 0.02 s interval. (frame rate: 400 fps) | 138 |

| | | |
|-------------|---|-----|
| Figure 4.30 | The images of bubble attachment on the membrane surface at 60 L/min air flow, (a) without vacuum, (b) with vacuum condition. (frame rate: 400 fps)..... | 139 |
| Figure 4.31 | Theoretical analysis of the net force acting on the foulants under different air flow rates..... | 141 |
| Figure 4.32 | (a) Flux performance and (b) normalized flux obtained for the S-VMD experiments over 60 h using marine diatom microalgal suspension as feed at 333 K under stagnant and continuous bubbling of 30 L/min. | 143 |
| Figure 4.33 | SEM-EDX analysis of the surface of (a) pristine membrane and fouled membranes using marine diatom microalgal suspension as feed at temperature of 333 K under the mode of stagnant (left) and continuous bubbling at 30 L/min (right) at (b) 15 h, (c) 30 h, (d) 45 h and (e) 60 h of S-VMD operation (magnification: 5,000× and 15,000×). | 144 |
| Figure 4.34 | SEM Microscopic structure change of marine diatom microalgae <i>Cylindrotheca fusiformis</i> sp. in the feed solution of 333 K over (a) 15 h, (b) 30 h, (c) 45 h and (d) 60 h of S-VMD operation (magnification: 40×)..... | 147 |
| Figure 4.35 | SEM-EDX analysis of cross section of used membrane after 60 h running S-VMD using marine diatom microalgal suspension as feed at temperature of 333 K under the mode of (a) stagnant and (b) continuous bubbling at 30 L/min (magnification: 5,000×)..... | 149 |
| Figure 4.36 | FTIR spectra of fresh and fouled hollow fibre membranes after 15, 30, 45 and 60 h running S-VMD using marine diatom microalgal suspension as feed at temperature of 333 K under stagnant and 30 L/min continuous bubbling condition. | 150 |
| Figure 4.37 | Pore size distribution (PSD) of fresh and fouled membranes after 60 h running S-VMD using marine diatom microalgal suspension as feed at temperature of 333 K under stagnant and 30 L/min continuous bubbling condition..... | 152 |

| | | |
|-------------|--|-----|
| Figure 4.38 | (a) Polysaccharides and (b) protein content on the fouled hollow fibre membranes over 15, 30, 45 and 60 h running S-VMD using marine diatom microalgae as feed at temperature of 333 K under stagnant and bubbling condition. | 153 |
| Figure 4.39 | Zeta potential values of microalgal feed solution over 60 h of S-VMD operation at temperature of 333 K. | 155 |
| Figure 4.40 | The temporal variation of water contact angle of pristine and fouled membranes over 60 h of S-VMD operation using non-bubbling and bubbling feed at temperature of 333 K. | 156 |
| Figure 4.41 | 3D AFM images of (a) fresh and fouled membranes under (b) stagnant feed, and (c) bubbling feed over 60 h of S-VMD operation at temperature of 333 K - analytical windows $20 \times 20 \mu\text{m}^2$ | 157 |
| Figure 4.42 | (a) Flux performance and (b) normalized flux obtained for the S-VMD experiments over 336 h and resumed 8 h operation after ultrasonic cleaning the membrane using marine aquaculture water as feed at 333 K under continuous bubbling of 30 L/min. | 159 |
| Figure 4.43 | SEM-EDX analysis of surface of (a) fouled membrane over 336 h operation (b) ultrasonic-cleaned membrane and (c) reused cleaned membrane over 8 h operation using marine aquaculture water as feed at temperature of 333 K under 30 L/min continuous bubbling enhanced S-VMD system (magnification: 5,000 \times). | 161 |
| Figure 4.44 | SEM of cross-sectional image of (a) fouled membrane over 336 h operation (b) ultrasonic-cleaned membrane and (c) reused cleaned membrane over 8 h operation using marine aquaculture water as feed at temperature of 333 K under 30 L/min continuous bubbling enhanced S-VMD system (magnification: 5,000 \times). | 162 |
| Figure 4.45 | FTIR spectra of fresh, fouled, cleaned and reused membrane over long term operation of air bubbling S-VMD system using marine aquaculture water as feed at temperature of 333 K under 30 L/min continuous bubbling condition. | 163 |

| | | |
|-------------|--|-----|
| Figure 4.46 | XRD spectra of fresh, fouled, cleaned and reused membrane over long term operation of air bubbling S-VMD system using marine aquaculture water as feed at temperature of 333 K under 30 L/min continuous bubbling condition..... | 165 |
| Figure 4.47 | Pore size distribution (PSD) of fresh, fouled, cleaned and reused membrane over long term operation of air bubbling S-VMD system using marine aquaculture water as feed at temperature of 333 K under 30 L/min continuous bubbling condition..... | 166 |
| Figure 4.48 | (a) Total energy consumption and (b) specific energy consumption in the air bubbling associated S-VMD desalination process over 40 h operation using a feed solution of 4.07 g/L Na ₂ SO ₄ and 5.84 g/L MgCl ₂ in 3.5 wt.% NaCl at 333 K. | 168 |
| Figure 4.49 | The predicted and average experimental <i>GOR</i> values at constant feed circulation rate of 0.9 L/min and continuous air flow of 30 and 60 L/min using synthetic salt solution and marine aquaculture water as feed at temperature of 333 K for the air bubbling S-VMD system using four hollow fibres. | 170 |

LIST OF SYMBOLS

| | |
|------------------|--|
| A_o | Outer surface area of the hollow fibre (m ²) |
| b | Thickness of the membrane (m) |
| C_{pL} | Specific heat capacity of feed (J/kg K) |
| $C_{p,w}$ | Specific heat capacity of water (J/kg K) |
| D | Bubble width flow (m) |
| d | Mean pore size of the membrane (μm) |
| d_c | Collision diameter of water vapour (m) |
| d_{cr} | Critical diameter of foulants (μm) |
| d_e | Equivalent diameter of hollow fibre in square pitch layout (m) |
| D_i | Inner diameter of the feed tank (m) |
| d_o | Outer diameter of hollow fibre (m) |
| d_p | Foulant size (m) |
| ε | Porosity of the membrane (%) |
| E_{in} | Total power input to the system (kW) |
| F_D | Drag force (N) |
| $F_{D,x}$ | Horizontal drag force (N) |
| F_L | Lift force (N) |
| $F_{L,x}$ | Horizontal lift force (N) |
| $F_{N,x}$ | Net normal force (N) |
| H_{latent} | Latent heat of the vaporization (J/kg) |
| $H_{latent,g,l}$ | Latent heat of the vaporization at two-phase feed (J/kg) |

| | |
|-------------------|--|
| h_T | Convective heat transfer coefficient in feed side (W/m ² K) |
| $h_{T,g,l}$ | Convective heat transfer coefficient in two-phase feed side (W/m ² K) |
| J | Theoretical flux (kg/m ² h) |
| J_p | Experimental flux (kg/m ² h) |
| k | Boltzmann constant (J/K) |
| k_L | Thermal conductivity of feed (W/m K) |
| k_m | Thermal conductivity of the membrane (W/m K) |
| K_n | Knudsen number |
| l | Mean free path of the transferred water vapour molecules (μm) |
| L | Length of hollow fibre (m) |
| M | Molar mass of water (kg/mol) |
| \dot{m}_{air} | Air flow rate (m ³ /s) |
| \dot{m}_f | Feed flow rate (m ³ /s) |
| \dot{m}_w | Water flow rate in the coil (m ³ /s) |
| N_f | No. of hollow fibres in the feed tank |
| N_K | Mass transfer via Knudsen diffusion (kg/m ² s) |
| η_{pump} | Pump efficiency (%) |
| Nu | Nusselt number |
| $Nu_{g,l}$ | Nusselt number at two-phase feed |
| ΔP | Pressure difference between membrane surface and permeate interfaces (Pa) |
| P_{atm} | Atmospheric pressure (Pa) |
| $P_{chiller}$ | Refrigerated bath power (kW) |
| ΔP_{circ} | Pressure difference to drive the circulation line (Psi) |

| | |
|-------------------|--|
| $P_{circulation}$ | Feed circulation pump power (kW) |
| P_{fm} | Partial pressure of water vapour at the outer surface of the membrane (Pa) |
| ρ_g | Density of air (kg/m ³) |
| ρ_L | Density of feed (kg/m ³) |
| Pr | Prandtl number based on T_f |
| Pr_s | Prandtl number based on T_{fm} |
| P_t | Tube pitch between adjacent hollow fibres (m) |
| ρ_w | Density of water (kg/m ³) |
| P_{vac} | Vacuum pressure in permeate side (Pa) |
| P_{vacuum} | Vacuum pump power (kW) |
| q_o | Air flow rate to be removed from the permeate line (ft ³ /min) |
| Q_{S-VMD} | Overall heat transfer (W) |
| R | Universal gas constant (m ³ Pa K) |
| r | Pore radius of membrane (m) |
| Re | Reynold number |
| Re_b | Reynold number of bubble flow |
| $Re_{g,l}$ | Sum of liquid and gas Reynold number |
| S | Salinity level (g/kg) |
| τ | Tortuosity factor of the pores |
| τ_s | Shear stress induced by bubble flow (Pa) |
| ΔT_{coil} | Temperature difference of the coil that provide heat flux (K) |
| T_f | Feed bulk temperature (K) |
| T_{fm} | Outer surface temperature of membrane (K) |

| | |
|---------------|---|
| $T_{f,m,g,l}$ | Outer surface temperature of membrane at two-phase feed (K) |
| T_m | Mean temperature of the pore (K) |
| T_{vac} | Saturated temperature at vacuum pressure (K) |
| μ_g | Viscosity of air (kg/m s) |
| μ_L | Viscosity of feed (kg/m s) |
| μ_w | Viscosity of water (kg/m s) |
| v | Feed stream velocity (m/s) |
| \bar{v} | Mean upward velocity based on rising bubble flow (m/s) |
| v_g | Velocity of air (m/s) |

LIST OF ABBREVIATIONS

| | |
|------------|---|
| AA | Alginic acid |
| AAS | Atomic absorption spectroscopy |
| AFM | Atomic force microscopy |
| AGMD | Air gap membrane distillation |
| AOM | Algogenic organic matter |
| ATR-FTIR | Attenuated Total Reflectance Fourier Transform Infrared |
| BSA | Bovine serum albumin |
| COD | Chemical oxygen demand |
| DCMD | Direct contact membrane distillation |
| EPS | Exopolymeric substances |
| EDX | Energy dispersive X-ray |
| FO | Forward osmosis |
| <i>GOR</i> | Gained output ratio |
| HA | Humic acid |
| LEP | Liquid entry pressure |
| MD | Membrane distillation |
| MED | Multi-effect distillation |
| MF | Microfiltration |
| MLVSS | Mixed liquor volatile suspended solids |
| MSF | Multi-stage flash |
| NOM | Natural organic matter |
| NF | Nanofiltration |
| PP | Polypropylene |
| PRO | Pressure retarded osmosis |
| PSD | Pore size distribution |
| PTFE | Polytetrafluoroethylene |
| PVDF | Polyvinylidene fluoride |
| RO | Reverse osmosis |
| <i>SEC</i> | Specific energy consumption |
| SEM | Scanning electron microscopy |
| SGMD | Sweeping gas membrane distillation |

| | |
|--------|--|
| S-DCMD | Submerged direct contact membrane distillation |
| S-VMD | Submerged vacuum membrane distillation |
| S-VMDC | Submerged vacuum membrane distillation and crystallization |
| TDS | Total dissolved solids |
| TEM | Transmission electron microscopy |
| TEPs | Transparent exopolymer particles |
| TPC | Temperature polarization coefficient |
| TOC | Total organic carbon |
| TSS | Total suspended solids |
| UF | Ultrafiltration |
| VMD | Vacuum membrane distillation |
| XRD | X-ray diffraction |

LIST OF APPENDICES

| | |
|------------|---|
| Appendix A | Marine aquaculture water sampling site |
| Appendix B | Preparation of f/2 medium recipe |
| Appendix C | Evaluation of membrane performance in S-VMD |
| Appendix D | Determination of cell counts for marine microalgal suspension |
| Appendix E | Calibration curves of synthetic feed solutions and marine aquaculture water |
| Appendix F | Measurements for bubble flow activity on membrane surface |
| Appendix G | Calculation of the quantification of EPS fouling layer on the membrane surface |
| Appendix H | Procedures for marine aquaculture water and permeate quality measurements using Lovibond digital photometer |
| Appendix I | Determination of membrane surface temperature in air bubbling S-VMD system |
| Appendix J | Determination of <i>GOR</i> values for air bubbling S-VMD system |
| Appendix K | Permeate quality test report over S-VMD desalination of marine aquaculture water |

**PENYULINGAN MEMBRAN VAKUM TENGGELAM UNTUK
PENYAHGARAMAN AKUAKULTUR AIR LAUT**

ABSTRAK

Penyulingan membran vakum (VMD) telah dianggap sebagai teknologi penyahgaraman yang menjanjikan dalam penghasilan air tawar. Penyahudaraan membran dengan cara vakum dalam sistem VMD konvensional cenderung mendorong memberi daya penggerak yang lebih tinggi dalam mencapai fluks resapan yang sangat baik. Dalam sistem VMD konvensional, bekalan haba luaran boleh mengakibatkan kehilangan haba yang lebih besar. Oleh itu, penyulingan membrane vakum tenggelam (S-VMD) secara kelompok dan bekalan haba dalaman diperkenalkan dalam projek ini. Sistem S-VMD berskala kecil bermanfaat untuk membekalkan air tawar kepada komuniti ladang akuakultur laut yang mempunyai ruang terhad di Malaysia. Sebatian bukan organik dan kehadiran mikroalga yang tidak dikehendaki dalam air akuakultur laut menyebabkan pengotoran membran yang ketara. Dalam kajian awal, pengotoran membran didapati didominasi oleh hablur berasaskan magnesium pada suhu suapan melebihi 333 K. Bahan organik yang merupakan bahan polimer ekstraselular (EPS) yang dirembes oleh mikroalga laut juga dijumpai di permukaan membran. Untuk menilai kebolehlaksanaan pemisahan dan prestasi energetik sistem S-VMD dalam penyahgaraman, prestasi sistem telah disimulasikan secara teori dan disahkan dengan baik oleh hasil eksperimen berasaskan pelbagai parameter operasi. S-VMD dapat berfungsi sebagai alternatif untuk VMD konvensional dengan mencapai fluks dan nilai nisbah ganda pengeluaran (GOR) yang setanding dengan sumber literatur. Untuk mencapai garis asas fluks dan GOR teori seperti yang disimulasikan dalam kajian berangka, penggelembungan udara digunakan dalam suapan untuk mengurangkan

kotoran bukan organik dan organik. Penggelembungan udara yang berterusan pada kadar aliran 30 L/min memberikan penyentalan permukaan yang berkesan untuk meminimumkan pemendapan hablur bukan organik dan EPS pada permukaan membran. Penggelembungan berterusan pada 30 L/min menunjukkan kecekapan pembersihan yang lebih baik dan mempunyai penggunaan tenaga khusus (SEC) yang hampir malar sepanjang operasi jangka panjang. Dalam operasi jangka panjang selama 336 jam menggunakan air akuakultur laut sebagai suapan, tidak ada pembasahan membran yang ketara berlaku dengan penolakan garam yang tinggi melebihi 99%. Hasil resapan memenuhi kualiti air mentah. GOR yang diperolehi dari sistem S-VMD yang dipertingkatkan dengan penggelembungan adalah 0.23, terutamanya disumbangkan oleh fluks yang stabil dan kecekapan pembersihan yang lebih baik. Dijangkakan sistem S-VMD ini dapat diterapkan di ladang akuakultur laut untuk menghasilkan air tawar bagi komuniti penternakan ikan tersebut.

SUBMERGED VACUUM MEMBRANE DISTILLATION (S-VMD) FOR MARINE AQUACULTURE WATER DESALINATION

ABSTRACT

Vacuum membrane distillation (VMD) has been recognized as a promising desalination technology to harvest freshwater. The deaerated pores of membrane by means of vacuum in conventional VMD system tend to promote higher driving force in achieving excellent permeate flux. In a conventional VMD system, external heat supply could result in greater heat loss. Therefore, a batch submerged VMD (S-VMD) with internal heat supply was introduced in this work. The small-scale S-VMD system is beneficial to supply freshwater to the community of space-limited marine aquaculture farm in Malaysia. Inorganic compounds and nuisance microalgae in marine aquaculture water caused noticeable membrane fouling. In a preliminary study, magnesium-based crystals were dominantly fouled on the membrane at feed temperature beyond 333 K. Organic matter which is extracellular polymeric substance (EPS) that secreted by the marine microalgae was also found on the membrane surface. To evaluate the feasibility of separation and energetic performance of the S-VMD system for desalination, the system performance had been theoretically simulated and validated well with the experimental results using various operational parameters. S-VMD could serve as an alternative to conventional VMD as the flux and gained output ratio (*GOR*) values are comparable with literatures. To achieve the baseline of theoretical flux and *GOR* as simulated in the numerical study, air bubbling was employed in the feed to mitigate the inorganic and organic fouling. Continuous air bubbling at a flow rate of 30 L/min provides effective surface scour to minimize inorganic crystals and EPS deposition on the membrane surface. Continuous bubbling

at 30 L/min showed better cleaning efficiency and had almost constant specific energy consumption (*SEC*) over long-term operation. In the long-term operation over 336 h using marine aquaculture water as feed, no apparent membrane wetting was occurred with high salt rejection above 99%. The permeate met the quality standard of raw water. The obtained *GOR* of the air bubbling enhanced S-VMD system was 0.23, mainly contributed by stable flux and better cleaning efficiency attained. Anticipatedly, the S-VMD system can be applied in the marine aquaculture farm to produce freshwater for the fisheries community.

CHAPTER 1

INTRODUCTION

This chapter provides an overview of the background of this research project. The scenario on freshwater footprint for marine aquaculture and submerged vacuum membrane distillation (S-VMD) process for marine aquaculture water desalination are introduced in Section 1.1. Based on the recent research studies in literatures, the problem statements of this work are addressed in Section 1.2 while research objectives of this work are formulated in Section 1.3. Finally, Section 1.4 presents the scope of this study and Section 1.5 outlines the thesis organization.

1.1 Research background

Our Earth covers 70% of water, approximately 332 million cubic miles, over 97% is seawater and only 3% is freshwater (Fukuzumi et al., 2017). Clean freshwater is essential to sustain a healthy human life. There are nearly 1.1 billion people in the world who have lack accessibility to water and 2.7 billion people who experience water shortage at least one month per year (World Wildlife Fund, 2021). According to World Wildlife Fund (2021), by 2025, two-thirds of the world's population will face water scarcity. It has been increasingly challenging to access freshwater in remote areas due to uneven water distribution and climate change. According to World Health Organization (2019), eight out of ten people in rural areas are still lacking basic water service in 2017, nearly half of them living in the least developed countries. The climatic factor, i.e. low rainfall, droughts, geological factor, overexploitation of groundwater as well as small catchment and space-limited areas will also cause water poverty in islands. Until recently, many islands are still relying on expensive water transfers from the mainland. Water transfer is usually done by sea transport, e.g. large

boats or tankers, and some people on islands who travel by boat or canoe. Marine aquaculture farm is one of the space-limited arid areas. The clean on-farm freshwater is essential to the livelihood of coastal fisheries community. Basically, marine aquaculture farm has limited space for clean water storage. The communities usually travel to mainland to access the freshwater for various on-sea human activities.

In global, 97% of the water comes from the sea. Hence, there is a need to devise a desalination process to obtain freshwater from abundantly available seawater. Desalination technology has advanced significantly in recent years with two conventional methods being increasingly deployed such as pressure driven reverse osmosis (RO) and multi-stage flash distillation (MSF). In RO, seawater is pumped through a series of membrane filtration process e.g. microfiltration (MF), ultrafiltration (UF) and nanofiltration (NF) to remove salts and minerals. While MSF employs heat to evaporate water and leave salt behind. Other membrane-based desalination technologies, such as osmotic driven forward osmosis (FO) and pressure retarded osmosis (PRO) as well as thermal processes such as membrane distillation (MD) are touted as promising technologies (Duong et al., 2020, Curto et al., 2021).

MD is one of the sustainable thermal-driven membrane separation technology. It is operated by means of vapour permeation through the microporous hydrophobic membrane to produce distilled water from seawater (Alsebaei and Ahmad, 2020, Hussain et al., 2021). The volatile vapour molecules like water are evaporated and diffused through the membrane to the permeate side as a result of the partial vapour pressure gradient. MD requires lower operating temperature than conventional thermal distillation process such as MSF and multi-effect distillation (MED). MD technology is capable in treating high saline water without compromising excellent salt rejection as it is not affected by the osmotic pressure gradient (Hardikar et al., 2020).

There are four different configurations of MD namely direct-contact membrane distillation (DCMD), vacuum membrane distillation (VMD), air gap membrane distillation (AGMD) and sweeping gas membrane distillation (SGMD). Amongst the MD process, VMD process produces higher flux than DCMD (Criscuoli et al., 2008, Cerneaux et al., 2009, Meng et al., 2015a). The vacuum created in the permeate side deaerates membrane pores. This helps to reduce the mass transfer resistance of water vapour and improve permeate flux, at the same time reducing the operation time. However, this conventional VMD configuration requires circulating heat supply across the membrane module with housing which induce excessive heat loss, consequently limiting the thermal efficiency of the system.

These drawbacks can be eliminated by operating the VMD as submerged VMD (S-VMD) in which hollow fibre membranes are immersed in the feed tank. The submerged MD is easy to be installed and constructed in a space-saving design, in which is suitable for small to large-scaled system at off-grid remote area and or for space-constricted site. In addition, installing heater in the feed tank for direct heat transfer can minimize heat losses in submerged MD system and enhance the feed flow across the membranes boundary layer through the natural convection currents by the heater, consequently ensuring uniform feed temperature and better total heat stored in the tank. These advantages render the future development of submerged MD in larger scale (Gryta, 2020).

However, the drawback of submerged MD is the induction of temperature and concentration polarization due to the difficulty of achieving high flow turbulence on the feed side. Assembling the heater in the submerged MD module allows the feed flow across the membrane bundle only by natural convection. Several works that employed mechanical agitation have been recently reported in submerged MD process

to reduce the negative polarization effects by generating forced convection to further enhance the flow turbulence at feed-membrane interface (Meng et al., 2015a, Julian et al., 2016, Julian et al., 2018b, Zhong et al., 2018, Zou et al., 2018, Gryta, 2020). According to Gryta (2020), the efficiency of multiple U-shaped S-DCMD membrane module and thermal efficiency could be improved by over 20%, respectively with the presence of mechanical mixing in the feed tank.

Besides, marine aquaculture water comprised high total dissolved solids (TDS) that contributed by seawater composition, nuisance algal blooming and organic matter which attribute to the periodical feedstock residues. These compounds are detrimental to membrane fouling, especially in the thermal operation of S-VMD. The vacuum applied in S-VMD system might induce serious pore blocking, consequently causing wetting and permeate contamination. Therefore, the application of marine aquaculture water in S-VMD for desalination requires further attention. Recently, the application of air bubbling has been gained attention in MD process for fouling control. Some studies claimed that the surface shear of air bubbles not only reduces the temperature polarization by improving hydrodynamic condition on the vicinity of membrane, but also scours the foulants away from the membrane (Ding et al., 2011, Chen et al., 2013, Wu et al., 2015). Nonetheless, long air bubbling operation in the MD system might promote the cooling of feed solution and attribute to lower driving force for vapour transport as a result of partial pressure reduction at feed side. Additional thermal energy is required for heating the feed solution. Besides, dissolved air and water vapour might compete each other for pore diffusion in the low-pressure environment of VMD system.

1.2 Problem statements

The poor mixing region at feed-membrane interface will cause temperature polarization inevitably in S-VMD system, creating big temperature difference between bulk feed and membrane surface (Anvari et al., 2020). As a result, the temperature-dependent driving force for vapour transport through the membrane is reduced. The temperature of feed-membrane interface should be kept as close to bulk temperature to ensure uniform heat flux and efficient water evaporation rate through the membrane boundary layer. Previous published works mainly focused on the heat transfer improvement by performing qualitative experimental studies using different turbulence approaches in S-VMD (Meng et al., 2015a, Zou et al., 2018, Zou et al., 2019, Bamasag et al., 2021). Further investigation on the numerical study of the process efficiency of S-VMD is needed to predict the theoretical flux and quantify the forced convective heat transfer coefficient as well as temperature polarization across a bank of the hollow fibre membrane boundary layer.

Despite the MD studies have been widely reported in recent years, membrane fouling, particularly inorganic fouling due to crystalline salts deposition on the membrane surface, remains one of the major obstacles for its future implementation in large scale. MD of seawater is susceptible to fouling due to high TDS. Membrane scaling is mainly caused by the sparingly soluble mixed salts such as calcium, magnesium, carbonate and sulphate in feed solution during MD desalination (Cheng et al., 2010, Curcio et al., 2010, Karanikola et al., 2018, Kim et al., 2020, Lee et al., 2020). These sparingly soluble mixed salts are inversely soluble at high temperature, thus potentially inducing salt precipitation and crystallization on the membrane surface. The deposition of scalants not only creates heat and mass transfer resistance, but also induces pore blocking and membrane wetting, and consequently deteriorating

the MD performance. Besides, higher vacuum degree in VMD might cause crystal intrusion to the inner pores of membrane. Producing freshwater for marine aquaculture farm is challenging as marine aquaculture water contains not only abundant inorganic salts, but also nuisance algal blooming due to excessive nutrient residues from the periodical feedstock. Microalgae secretes algogenic organic matter (AOM) during their growth. They are complex mixture of organic substances which mainly comprised of exopolymeric substances (EPS), which is also known as extracellular polymeric substances. These EPS are made up of carbohydrates and proteins that carry negative surface charge (Henderson et al., 2008). Significant EPS production increases with the increase of salinity to keep marine microalgae safe from the built-up osmotic pressure. Transparent exopolymer particles (TEPs) is abundant form of EPS which classified as organic particles that are predominantly made up of acidic polysaccharides, with the appearance of transparent gel-like sticky structure (Bilad et al., 2014). It is believed that the specific structure of TEPs could induce biofilm formation and colloidal fouling on membrane (Discart et al., 2013). Despite microbial growth is gradually retarded during MD process, the secretion of EPS by marine algae will be increased subjected to N- and P- nutrients depletion at high operating temperature (Magaletti et al., 2004). These organic matters would be expected to have high impact on fouling when the membrane is being exposed to algal bloom and marine aquaculture water. Therefore, further investigation on the sparingly soluble mixed salts of seawater and the high loads of marine microalgal cells and EPS secretion towards the fouling propensity of membrane in S-VMD system is needed.

Few recent studies have introduced gas bubbling to mitigate fouling and improve permeate flux in MD system (Ding et al., 2011, Chen et al., 2013). The presence of a gas-liquid two-phase flow improves the surface shear rate and promotes

turbulence flow near the membrane surface. This not only reduces the negative polarization effects, but also reduces foulant deposition on the surface membrane. However, Meng et al. (2015a) reported that the bubbling applied in the brine feed solution comprising sparingly soluble mixed salts caused membrane scaling in submerged VMD (S-VMD). Another study claimed that long bubbling duration in cross-flow DCMD significantly reduced the feed-membrane contact area and partial vapour pressure gradient across the membrane (Ding et al., 2011). The formation of long bullet-shaped slug bubbles could block the liquid flow passage across the membrane boundary layer more significant compared to fine bubbles. In addition, higher shear rate promoted by higher bubble flow might induce nucleation of salts and crystallization on the membrane surface (Mullin and Raven, 1961). These previous works which only reported qualitatively the use of bubbling in different MD configurations and feed compositions showed contradicted findings and most of the works do not quantify the bubble size and its activity on the membrane surface. Hence, a comprehensive study on optimum bubbling intensity in S-VMD is required to achieve efficient separation process and prevent fouling on the membrane. Further microscopic evaluation on the shear stress induced by bubble flow and bubble size is also required to provide comprehensive understanding of bubbling in mitigating fouling.

The internal heating of S-VMD design ensures better heat preservation for feed solution in the membrane-submerged tank. Anticipatedly, S-VMD could consume lower energy compared to conventional VMD which experiences greater heat loss from external heat supply. Meng et al. (2015a) reported S-VMD system for inland desalination has lower energy consumption than conventional VMD configuration. However, their studies are not reported in *GOR* or other quantitative efficiency

analysis. In addition, effective turbulence flow across the membrane boundary layer will provide surface shear for antifouling and at the same time enhancing permeate flux. However, the turbulence approach might be energy intensive to the system. By taking practical implementation of MD system as consideration, a good antifouling approach will lead to higher and more stable flux as well as constantly low *SEC* value over long operation. Therefore, it is notably interesting to investigate and quantify the energetic performance of S-VMD system, which could potentially be alternative to conventional VMD system. A comprehensive study on water productivity and energy requirement is also required to evaluate the antifouling S-VMD system.

This is the first attempt of this work to adopt the shell-and-tube heat exchanger concept in quantifying the forced convective heat transfer coefficient to drive vapour diffusion across a bank of the submerged hollow fibre membranes (tube side) in the tank (shell side) based on the equivalent diameter of the hollow fibres arranged in square pitch layout. Besides, this is the first attempt to provide a microscopical study of bubble activity on the membrane surface in S-VMD system. To the best of our knowledge, the application of marine aquaculture water desalination in S-VMD has never been studied. Based on the finding of this work, the S-VMD system can desalinate not only the marine aquaculture water that has high salt content but also the algal bloomed water.

1.3 Research objectives

The aim of this study is to design a S-VMD system with excellent transmembrane flux performance as well as NaCl and microalgae rejections for desalinating marine aquaculture water. The research objectives are formulated as below:

1. To assess and simulate the performance of S-VMD system based on different operating conditions.
2. To evaluate the fouling propensity of the S-VMD system towards inorganic scalants and microalgae.
3. To investigate the efficiency of air bubbling for fouling control in the S-VMD system and the bubble activity on the membrane surface microscopically.
4. To analyze the energy efficiency of the S-VMD system.

1.4 Scope of study

Firstly, a preliminary study was carried out to determine the critical fouling temperature and membrane selection. A marine aquaculture water jar test study was conducted at varied temperature between 298 to 343 K to determine the critical temperature that caused membrane fouling and identify the predominant foulants. Two commercial polypropylene (PP) hollow fibre membranes with hydrophobic nature were employed to compare their flux and fouling propensity in short-term S-VMD operation. The membrane with higher flux and pore blocking resistance (ACCUREL PP) was then assembled in a bundle of 4 fibres in 25 cm long (effective area of 0.0085m²) and used in the entire S-VMD experiments. Based on the membrane properties of ACCUREL PP, the theoretical flux and energetic performance of the S-VMD system were simulated and validated with the experimental results at varied feed temperature, feed circulation flow rate, and vacuum pressure at permeate side. The saline water, 3.5 wt.% sodium chloride (NaCl) solution was used as feed to evaluate the system at temperature of 328-338 K, circulation flow rates of 0.3-0.9 L/min, and vacuum pressure of 3-7 kPa. The setting of these parameters is based on the typical

3.5 wt.% salinity of seawater, predetermined critical fouling temperature of 333 K from the preliminary study, the capacity of the circulation pump and the critical vacuum degree that caused vapour pre-condensation at the inner tube of the hollow fibres as a result of the higher condensing saturation temperature which close to room temperature, respectively.

For the inorganic fouling and mitigation study, the transmembrane flux and salt rejection were monitored continuously for 40 h using a mixture of NaCl solution with magnesium sulphate (MgSO_4) salts which had been predetermined as the dominant scalant based on the marine aquaculture water jar test study, in the composition of 4.07 g/L sodium sulphate (Na_2SO_4), and 5.84 g/L magnesium chloride (MgCl_2) based on the typical compounds in the seawater. The flux performance was evaluated at feed temperature of 333 K under the mode of stagnant, circulation at 0.9 L/min, intermittent and continuous bubbling at 30 and 60 L/min, respectively. For the organic fouling control study, the permeate flux was monitored under continuous bubbling at 30 L/min and compared with stagnant feed for 60 h operation using a marine diatom algal culture *Cylindrotheca fusiformis* sp. with cell density of approximately 1.5×10^5 cells/mL suspending in 3.5 wt.% sea salt solution at temperature of 333 K. The S-VMD system was then performed in long-term operation of 14 days using real marine aquaculture water at bubbling rate of 30 L/min to evaluate its feasibility and practicality. Lastly, the energy efficiency of the bubbling S-VMD system was evaluated and compared at different bubbling rates with feed circulation mode.

1.5 Thesis organization

This thesis comprises of five chapters. The contents of each chapter are summarized as below:

In Chapter One, the overview on freshwater demand for marine aquaculture and membrane desalination technology using S-VMD is first provided. Next, based on the problems associated with marine aquaculture water desalination using S-VMD process, the problem statements are addressed with the formulation of research objectives. Lastly, this chapter is ended with the scope of study and thesis organization.

Chapter Two gives the comprehensive literature review on the recent research progress related to the current work. Firstly, freshwater demand and the characteristics of marine aquaculture water are reviewed. Principle of VMD configuration is then discussed. Next, the application of VMD in desalination and the comparison of submerged and conventional VMD are thoroughly discussed. Besides, the fouling phenomenon in MD and the fouling control strategy are discussed in detail. The energy efficiency of VMD process is also reviewed in detail on the aspect of specific energy consumption (*SEC*) and gained output ratio (*GOR*). Lastly, the challenges in the S-VMD desalination of marine aquaculture water are presented. The research gaps are also highlighted.

Chapter Three provides the list of the raw materials, chemicals and apparatus used in this project as well as the experimental flow chart. Besides, the experimental procedures are disclosed in detail with their purpose, including S-VMD experimental set-up in evaluating membrane performance, marine aquaculture water and permeate water quality analysis, and membrane characterizations. The simulation procedures for developing S-VMD model are also discussed with the support of theoretical analysis.

Chapter Four reveals the important findings of this work based on the addressed research objectives. The critical temperature and major foulants that triggered fouling based on the preliminary marine aquaculture jar test study are first reported. Next, the two commercial membranes in short term S-VMD operation are

compared with focus on the fouling propensity and the selection of membrane for long term use in S-VMD operation. This is then followed by the findings on the theoretical flux and energetic performance of the S-VMD system obtained from simulation and validation of the experimental data. Besides, the role of air bubbling take place in scaling and microalgal fouling is presented. The findings on the separation performance of membrane and structural characteristics of scalants and EPS that released from microalgal cells are subsequently provided and supported by characterization. This chapter is ended with the finding on the long term run of S-VMD performance for desalination of real marine aquaculture water which focus on the key requirements: permeate flux, membrane reusability, permeate quality and energy consumption.

Lastly, Chapter Five summarizes the major findings of this study according to the developed research objectives. Few recommendations are suggested to improve the future works based on the current research findings.

CHAPTER 2

LITERATURE REVIEW

This chapter summarizes the latest development of research related to the current project. Section 2.1 introduces the characteristics of marine aquaculture water. Next, Section 2.2 discusses the past development of conventional and submerged VMD in desalination process. Besides, Section 2.3 and Section 2.4 review the latest progress of fouling phenomenon and control strategies introduced in conventional and submerged MD configurations. After that, Section 2.5 discusses the literatures of the energy consumption of conventional and submerged VMD for desalination. In Section 2.6, the desalination of marine aquaculture water using S-VMD process is highlighted with the discussion on the current challenges faced by previous studies. Finally, the research gaps are discussed in Section 2.7.

2.1 Marine aquaculture

Recently, arising from the increase of world population about 2.2 billions people from 1986 to 2018, fish proteins are in pressing needs to fulfil the yearly consumption. The rapid development of aquaculture sector contributed to an increase in total fish production from 14.9 to 82.1 million tonnes per year (Food and Agriculture Organization, 2020). Marine and coastal aquaculture significantly produced 30.8 million tonnes (USD 106.5 billion) of aquatic animals in 2018. According to Food and Agriculture Organization (2020), the marine aquaculture in Malaysia produced 45.9 thousand tonnes of crustaceans in 2018. Since the coastal ponds for aquaculture are found more concentrated in South, Southeast and East Asia, the livelihood and economic development among coastal communities requires freshwater for direct consumption. Besides, 4.25 million tonnes of agriculture crops used in the feeds for

marine aquaculture production had resulted in an indirect total water footprint of 8 km³ per year (Troell et al., 2014).

The marine water quality is highly dependent on the waves, water tide and aquaculture activities (Zhang et al., 2020). The marine water quality may be deteriorated due to continuous waste discharge from industry and domestic sewage, as well as untreated effluent from aquaculture. The seasonal rainfall and water tide will fluctuate the salinity of marine water. Nitrate is mainly derived from aquaculture activities and wastewater effluent. Salinity variation led to the changes of microbial function and the process of nitrification and denitrification, thus affecting ammoniacal nitrogen concentration in water. The rainfall could promote the growth of plankton by supplying oxygen, which encourage the absorption of nutrients. Temperature affects phytoplankton growth by affecting photosynthesis and phosphorus concentration. The low-intense sunlight will reduce the photosynthesis of algae and oxygen production. Furthermore, the degradation of organic matter from dead phytoplankton cells also highly consumed oxygen, which may cause the water pollution and eventually affecting the aquaculture production.

There are some constraints for marine aquaculture farm to access freshwater supply. The main problem is the limited rainwater catchments. Rainwater harvesting from rooftops is normally practised in small islands and marine farming (Hophmayer-Tokich and Kadiman, 2006). Nevertheless, rainwater harvesting could not be treated as the main source of water supply to the space-limited marine aquaculture farm due to limited supply and uncertain seasonal rainfall over the years. Therefore, desalination is required to purify marine water in order to obtain consistent freshwater supply for the marine aquaculture farm. The most common desalination technology is pressure driven RO process. The high operating pressure of RO with a series of membrane

filtration process is energy intensive, which poses certain limitation to the energy-deprived marine aquaculture farm. Recently, MD is touted as one of the promising desalination technologies. A clean water can be obtained by operating MD at temperature range of 323-353 K. The low operating temperature requirement promotes the coupling of MD with renewable energy, i.e. solar which is accessible in marine aquaculture farm (Lu et al., 2019b, Ma et al., 2020, Chen et al., 2021, Miladi et al., 2021). Furthermore, hydrophobic hollow fibres used in MD pose high membrane surface areas per unit volume that potentially yield high permeate flux in the confined membrane module (El-Zanati et al., 2021). Amongst the MD process, VMD process produces higher flux than DCMD. The vacuum at the permeate side of VMD efficiently removes air within membrane pores, contributing to greater driving force for water vapour transport.

2.2 Application of VMD for desalination

2.2.1 Principle of VMD

VMD is thermal driven process that involves phase change. The feed solution flows across the surface of a microporous hydrophobic membrane and water vapour diffuses into the membrane pores at the feed-membrane interface. The water vapour is then externally condensed as distillate or permeate under vacuum condition. Basically, the vacuum pressure which applied at the permeate side of the membrane is maintained below the saturation pressure of the volatile solutes to be separated from the hot feed solution. The driving force of the process is caused by the partial vapour pressure difference between the feed and permeate side of the membrane which is temperature dependence. Compared to DCMD, VMD has higher partial pressure gradients as a result of low pressure at permeate side, thus leading to higher permeate flux. In

addition, VMD has higher thermal efficiency as conductive heat loss through the membrane layer is nearly negligible (Fan and Peng, 2012).

2.2.2 Conventional and submerged VMD configurations used in desalination

Various works have been done to develop VMD for desalination, as shown in Table 2.1. The flux performance of superhydrophobic PVDF–PTFE electrospun nanofibrous composite flat-sheet membranes used in VMD process for desalinating 3.5 wt.% NaCl solution at feed temperature of 333 K under 1.5 L/min feed flow rate and the permeate pressure of 9 kPa surpassed the commercial PTFE membrane (18.5 vs 15 kg/m²h) due to its larger void volume fraction and interconnected open structure (Dong et al., 2014). Besides, compared with DCMD process, the synthesized thin PVDF flat-sheet membrane was found to be more suitably used in VMD process due to its higher thermal efficiency (88.1% vs 59.6%) and permeate flux (22.4 vs 19.0 kg/m²h) obtained with a NaCl rejection of 99.9% at a feed temperature of 346 K under 0.9 L/min feed flow and permeate pressure of 31.5 kPa (Fan and Peng, 2012). The efficiency of the VMD process using PVDF hollow fibre membrane with 5 wt.% brine solution could be increased by increasing the feed temperature, vacuum degree and feed flow rate. The maximum flux could be obtained at 14.1 kg/m²h at a feed temperature of 361 K under 2.7 m/min feed flow and permeate pressure of 20.3 kPa (Yan and Wang, 2017). In addition, the alumina hollow fibre which was synthesized via phase inversion, sintering and surface grafting with fluoroalkylsilane method achieved comparable performance with other polymer membranes via VMD process using 4 wt.% NaCl solution at 353 K and permeate pressure of 4 kPa, whereby flux of 42.9 kg/m²h and salt rejection over 99.5% were attained (Fang et al., 2012). A pilot test of VMD was conducted on the ship using waste-heat produced from the vessel engine to preheat seawater feed. The permeate flux achieved 5.4 kg/m²h with the salt

Table 2.1 Published literature reports about the application of VMD and S-VMD configurations in desalination.

| Material and type of membrane | Salt rejection (%) | Feed temperature (K) | Vacuum pressure (kPa absolute) | Feed flow (L/min) | Permeate flux (kg/m ² h) | Significant outcomes | References |
|--------------------------------|--------------------|----------------------|--------------------------------|-------------------|-------------------------------------|---|----------------------|
| PVDF–PTFE composite flat-sheet | 99.9 | 333 | 9 | 1.5 | 18.5 | The superhydrophobic PVDF–PTFE nanofibrous membrane performed better than commercial PTFE due to its larger pore size, LEP and contact angle. | (Dong et al., 2014) |
| PVDF flat-sheet | 99.9 | 346 | 31.5 | 0.9 | 22.4 | VMD had higher permeate flux and thermal efficiency compared to DCMD. | (Fan and Peng, 2012) |
| PVDF hollow fibre | 99.8 | 361 | 20.3 | 2.7 m/min | 14.1 | The efficiency of VMD can be improved by optimizing the feed flow rate, feed temperature and vacuum degree. | (Yan and Wang, 2017) |
| | 99.9 | 328 | 5 | N/A | 14.1 | The flux of S-VMD was found higher than that of S-DCMD. | (Choi et al., 2017) |
| Alumina hollow fibre | 99.5 | 353 | 4 | N/A | 42.9 | The membrane was prepared via the method of phase inversion extrusion, sintering and surface grating with fluoroalkylsilane. | (Fang et al., 2012) |

Table 2.1 Continued

| Material and type of membrane | Salt rejection (%) | Feed temperature (K) | Vacuum pressure (kPa absolute) | Feed flow (L/min) | Permeate flux (kg/m²h) | Significant outcomes | References |
|--------------------------------------|---------------------------|-----------------------------|---------------------------------------|--------------------------|--|--|-------------------------|
| PP hollow fibre | 99.99 | 328 | 8.3 | 8.3 | 5.4 | Low grade heat from the vessel engine was used to preheat seawater feed. | (Xu et al., 2006) |
| | 99.9 | 343 | 5 | N/A | 6.9 | The flux of S-VMD was achieved 6.9 kg/m ² h in pure water test without agitation. | (Julian et al., 2016) |
| | 99.9 | 343 | 10 | N/A | 6.0 | The flux of S-VMD was higher than that of S-DCMD in the absence of agitation. | (Meng et al., 2015a) |
| | 99.9 | 343 | 12 | N/A | 11.7 | Synthetic inland brine water which comprised 0.692 wt.% of NaCl, calcium chloride and sodium bicarbonate solution was used as feed in S-VMDC system. | (Julian et al., 2018a). |

Table 2.1 Continued

| Material and type of membrane | Salt rejection (%) | Feed temperature (K) | Vacuum pressure (kPa absolute) | Feed flow (L/min) | Permeate flux (kg/m²h) | Significant outcomes | References |
|--------------------------------------|---------------------------|-----------------------------|---------------------------------------|--------------------------|--|---|------------------------|
| PP hollow fibre | 99.9 | 343 | 5.0 | N/A | 11.0 | Inland brine model with TDS content of 3.28 wt.% was employed as feed in S-VMDC system. | (Julian et al., 2018b) |
| PTFE hollow fibre | 99.9 | 348 | 15 | N/A | 3.8 | 0.18 wt.% of aqueous calcium sulphate solution was used as feed in S-VMD. | (Zou et al., 2018) |
| | 99.9 | 348 | 15 | N/A | 6.3 | High S-VMD flux obtained in desalinating 10 wt.% of NaCl solution. | (Zou et al., 2019) |

retention of 99.99% at feed temperature of 328 K under 8.3 L/min flow rate and permeate pressure of 8.3 kPa (Xu et al., 2006).

However, the external heat supply of conventional VMD configuration might reduce the feed temperature due to heat loss experienced by the feed solution during pumping, hence limiting the thermal efficiency of the system. Recently, submerged MD has been increasingly gained much attraction in research for its future implementation in large scale. The S-VMD system could minimize heat loss as the hot feed solution with the presence of fully immersed membranes is stored in a tank of low aspect ratio (ratio of length to diameter) during operation (Choi et al., 2017). In addition, installing heater in the feed tank of S-VMD system for direct heat transfer could enhance the feed flow across the membrane boundary layer via natural convection currents from the heater, as a result ensuring uniform feed temperature and better heat storage in the tank (Gryta, 2020). Simulation results from the work of Dong et al. (2019) found that the low module aspect ratio (tank height/tank diameter) of S-VMD design encourages the industrial scale up due to its minimum axial heat loss compared to conventional DCMD and VMD configurations. The large feed tank diameter (>10 cm) could increase flux stability due to the improved heat stored in the tank.

The flux of S-VMD was found higher than that of S-DCMD using deionized water as feed at temperature of 328 K (14.1 vs 7.9 kg/m²h) as the vacuum applied at 5 kPa resulted in higher driving force for water vapour diffusion through the PVDF hollow fibre membranes (Choi et al., 2017). The flux of S-VMD was achieved 6.9 kg/m²h using PP hollow fibre membranes in pure water test without agitation at temperature of 343 K and permeate pressure of 5 kPa (Julian et al., 2016). Similarly, another study found that the flux of S-VMD was higher than that of S-DCMD in the

absence of agitation (8.2 vs 4.5 kg/m²h for pure water test, while 6.0 vs 3.0 kg/m²h for 20 wt.% NaCl solution test) using PP hollow fibre membranes at feed temperature of 343 K and permeate pressure of 10 kPa (Meng et al., 2015a). The flux of S-VMD was attained 3.8 kg/m²h using PTFE hollow fibre membranes with 0.18 wt.% of aqueous calcium sulphate solution as feed at temperature of 348 K and permeate pressure of 15 kPa (Zou et al., 2018). The flux of S-VMDC was attained at 11.7 kg/m²h using PP hollow fibre membranes with 0.692 wt.% of NaCl, calcium chloride and sodium bicarbonate solution as the synthetic inland brine water feed at temperature of 343 K and permeate pressure of 12 kPa (Julian et al., 2018a). In another S-VMDC study of using inland brine model as feed with higher TDS of 3.28 wt.%, the average permeate flux reached 11.0 kg/m²h at temperature of 343 K and permeate pressure of 5 kPa (Julian et al., 2018b). The attained flux of S-VMD was 6.3 kg/m²h using PTFE hollow fibre membranes with 10 wt.% of NaCl solution as feed at temperature of 348 K and permeate pressure of 15 kPa (Zou et al., 2019).

2.3 Fouling phenomenon in MD

Fouling is a phenomenon that allows the build-up of undesired materials on membrane surface (Laqbaqbi et al., 2019, Ravi et al., 2020). Generally, fouling materials consist of either living organisms or a non-living substance. Membrane surface or its pores will be blocked via accumulation, attachment or adsorption of foulants during mass transport of MD process. Fouling will cause permeate flux dropped especially in the long-term operation. The concept of fouling in MD process is illustrated in Figure 2.1. As seen in Figure 2.1(a), initial membrane fouling only happens on membrane surface by deposition or adsorption of foulants. At this initial stage, the water vapour flux can be maintained as there is available open pore area that

allows water evaporation to occur in the feed side. The deposits will then continuously cover the membrane pores, which partially or fully blocks the membrane pores as shown in Figures 2.1(b-d). Some pores are partially wetted or covered due to the attachment of hydrophilic foulants onto the inner wall of the pores. The fouling exacerbation affects the flow pattern of bulk feed and thus significantly increases the resistance of heat and mass transfer between the bulk feed and evaporation interface. As a result, the temperature and concentration polarizations are induced at the evaporation interface. Consequently, water vapour flux is declined due to smaller water vapour pressure gradient across the membrane. Besides, the polarizations will cause the vapour-liquid interface more supersaturated and gradually exhibit crystallization growth in the pores, which significantly lead to complete pore wetting toward the permeate side of the membrane, as illustrated in Figures 2.1(e) and (f). The marine water with high TDS which comprise sparingly soluble salts that are increasingly insoluble at higher temperature could cause the membrane used in MD process more susceptible to inorganic fouling. While the organic matters and microalgae in the marine aquaculture water which are attributed to the aquaculture activities could potentially cause organic fouling and biofouling to the membrane.

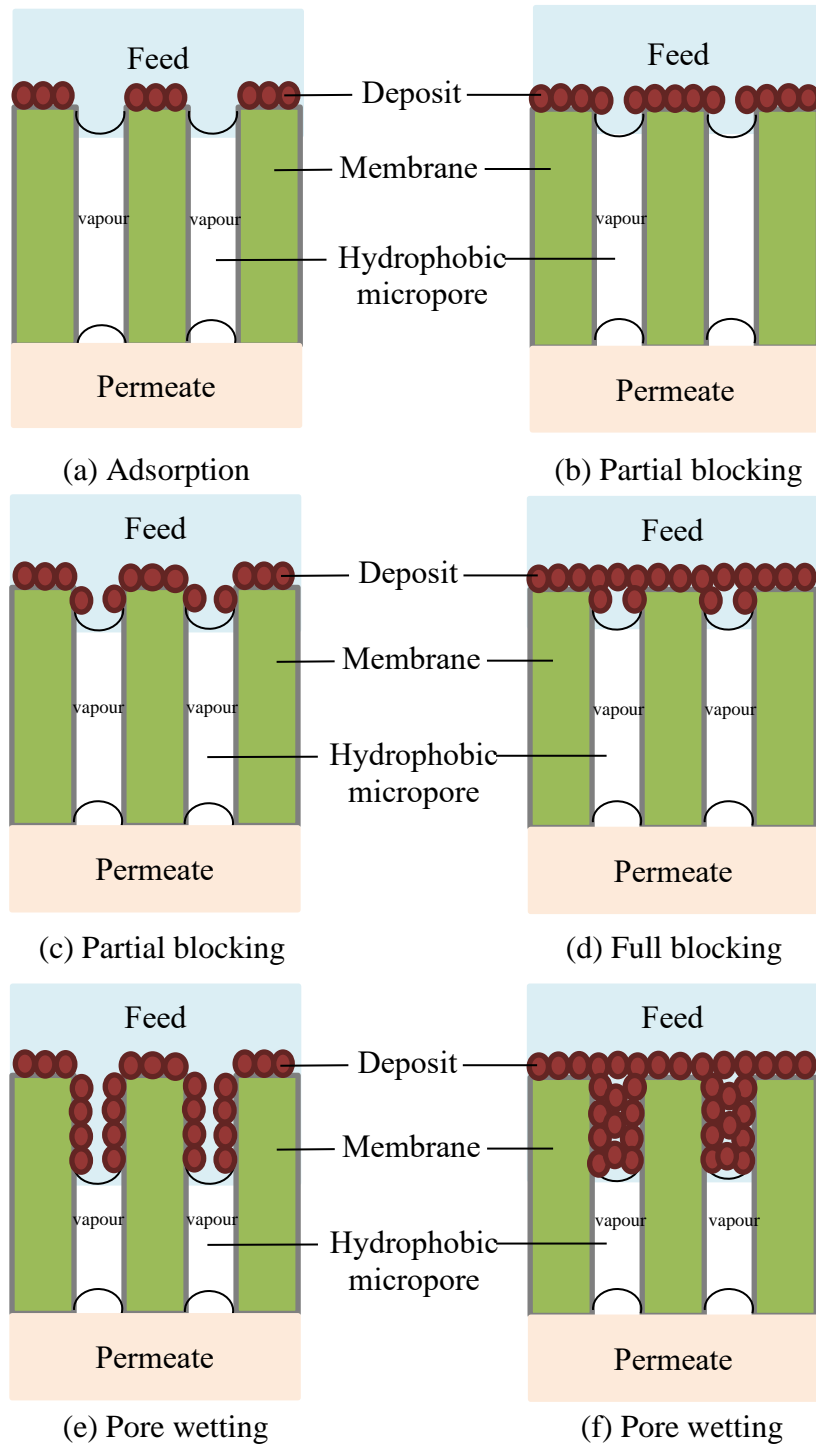


Figure 2.1 Types of membrane fouling in MD process.

2.3.1 Inorganic fouling

Inorganic fouling is generally known as scaling. It involves salt precipitation from feed solution deposited onto the membrane surface. Consequently, it affects the

water vapour transport across the membrane and significantly cause a flux reduction (Warsinger et al., 2015). Scaling occurs when supersaturation is reached due to water evaporation and temperature changes via crystallization growth on the membrane surface (van de Lisdonk et al., 2001). The scales tend to tackle the larger pores and consequently induce pore wetting as illustrated in Figures 2.1(e) and (f) (Tijing et al., 2015). Deposition of the crystal on the membrane surface will increase temperature polarization and consequently causing the permeate flux decline (Naidu et al., 2016). Common scales such as calcium sulphate (CaSO_4), calcium carbonate (CaCO_3) and MgSO_4 are widely found in water source like seawater.

Qin et al. (2018) reported that flux decline in VMD is higher than that of DCMD based on calcium carbonate fouling impact. This is because the decomposition of dissolved $\text{Ca}(\text{HCO}_3)_2$ in VMD is faster which shifts the reaction to the right to produce CaCO_3 upon CO_2 removal. Besides, the solubility of CaCO_3 is inversely proportional to temperature. High temperature of feed solution will induce CaCO_3 crystal formation. Pure CaCO_3 scales causes rapid flux decline up to 66% due to its non-porous nature (Karakulski and Gryta, 2005). However, higher feed flow rates will reduce crystallization growth and make the carbonate scales more porous and loosen (Gryta, 2008a). Besides, the penetration of CaCO_3 scales into the membrane pores could induce wetting and permeate contamination (Gryta, 2009). In addition, the needle-like gypsum CaSO_4 crystals are prevalent to penetrate into membrane pores, thus consequently, inducing pore wetting and membrane damage that could reduce the flux as much as 29% (Gryta, 2009). Naidu et al. (2014a) observed that a slight permeate flux decline (18–20%) by the loosely-deposited CaSO_4 crystals was found in the multi-effect VMD system after 920 min of operation under the conditions of